Supporting Information for

Quantitatively Mapping Cellular Viscosity with Detailed Organelle Information via a Designed PET Fluorescent Sensor

Tianyu Liu,[1,2†] *Xiaogang Liu,*[3†] *David R. Spring,*[4]* *Xuhong Qian,*[5]* *Jingnan Cui,*[2]* *and Zhaochao Xu*[1]*

[1] Dalian Institute of Chemical Physics, Chinese Academy of Sciences, Dalian 116023, China; [2] State Key Laboratory of Fine Chemicals, Dalian University of Technology, Dalian 116012, China; [3]Cavendish Laboratory, Department of Physics, University of Cambridge, UK; [4]Department of Chemistry, University of Cambridge, Lensfield Road, Cambridge, UK; [5]School of Pharmacy, East China University of Science and Technology, Shanghai 200237, China.

E-mail: zcxu@dicp.ac.cn; jncui@dlut.edu.cn; spring@ch.cam.ac.uk; xhqian@ecust.edu.cn

†Contributed equally to this work.

Contents

List of Figures

List of Tables

Materials and Methods

Unless otherwise stated, all reagents were purchased from Aldrich and used without further purification. ^{1}HNMR and ^{13}C-NMR spectra were recorded on a VARIAN INOVA-400 spectrometer, using TMS as an internal reference. Mass spectrometry data were obtained with a HP1100LC/MSD mass spectrometer and a LC/Q-TOF MS spectrometer. UV-visible spectra were collected on a Perkin Elmer Lambda 35 UV-Vis spectrophotometer. Fluorescence measurements were performed on a HITACHI F7000 Fluorescence Spectrophotometer.

Synthesis

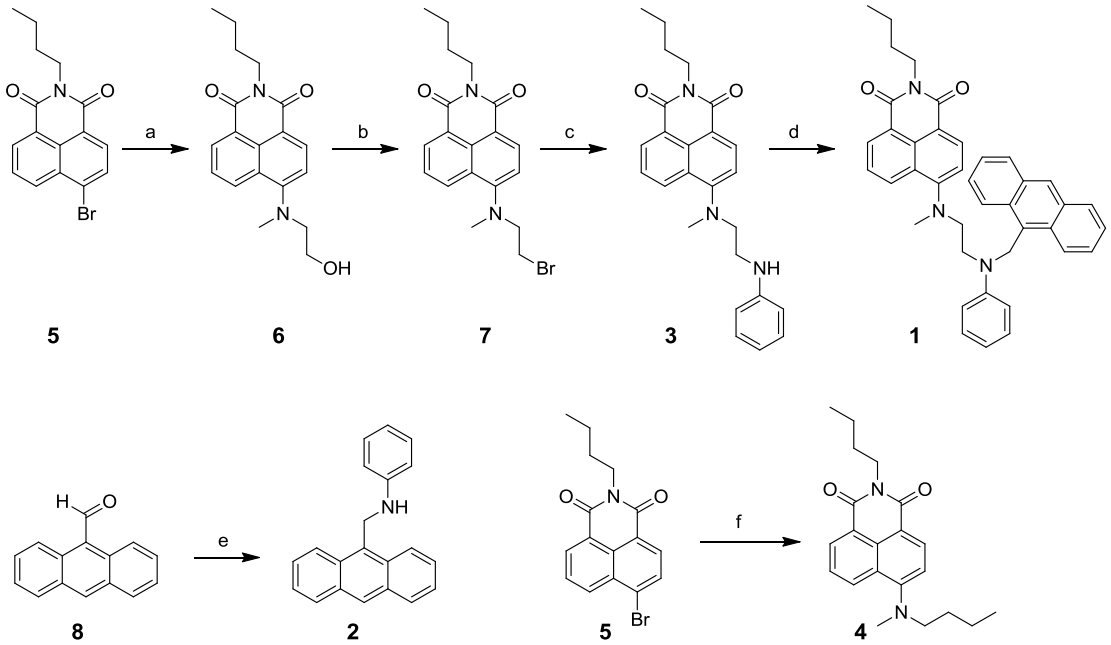

Scheme S1. Synthesis of compounds **1**—**4**. Reagents and conditions: (a) *N*-methylethanolamine, $CH_3OC_2H_4OH$, Et_3N, reflux, 75.2%; (b) PBr_3, CH_2Cl_2, RT, 71.1%; (c) aniline, $CH_3OC_2H_4OH$, Et_3N, reflux, 59.8%; (d) $CH_3OC_2H_4OH$, KI, Et_3N, N_2, reflux, 61.1%; (e) 9-Anthraldehyde，aniline，toluene; (f) *N*-methylpropylamine, ethanol.

Synthesis of 6. 4-Bromine-1,8-naphthalene anhydride (3.31 g, 0.01 mol), triethylamine (2.788 mL, 0.02 mol) and *N*-methylethanolamine (1.615 g, 0.02 mol) were dissolved in 20 mL 2-methoxyethanol. After refluxing for 24 h under nitrogen atmosphere, the reaction solution was cooled to room temperature and then poured into 50 mL ice water. The precipitate was filtered and the crude product was purified by column chromatography (SiO_2, PE:EA = 4:1, v/v) to give 2.45 g compound **6** in 75.2% yield. ^{1}H NMR (400 MHz, $CDCl_3$) δ 8.61 (d, *J* = 8.0 Hz, 1H), 8.58 (d, *J* = 8.0 Hz, 1H), 8.50 (d, *J* = 8.0 Hz, 1H), 7.69 (t, *J* = 8.0 Hz, 1H), 7.28 (d, *J* = 8.0 Hz, 1H), 4.17 (t, *J*

= 7.2, 2H), 3.96 (d, *J* = 5.6 Hz, 2H), 3.50 (t, *J* = 5.6 Hz, 2H), 3.08 (s, 3H), 2.05 (s,1H, OH), 1.71 (m, 2H), 1.43 (m, 2H), 0.97 (t, *J* = 7.2 Hz, 3H). HRMS (ESI) calcd for $C_{19}H_{23}N_2O_3$ [MH^+] 327.1709, found 327.1706.

Synthesis of 7. The solution of compound **6** (1.63 g, 5 mmol) in 20 mL CH_2Cl_2 was cooled to 0˚C followed by the slow addition of phosphorus tribromide (0.57 mL, 6 mmol). The solution was then warmed to 35˚C and stirred for 12h. After cooling to room temperature, the solution was washed with water (2×30 mL) and brine (2×30 mL) and dried over $MgSO_4$. The solvent was removed under reduced pressure. The product was then purified by gel column chromatography (SiO_2, PE:EA = 4:1, v/v) to give **7** as a yellow powder in 71.1% yield (1.38 g). 1H NMR (400 MHz, $CDCl_3$) δ 8.60 (d, *J* = 8.0, 1H), 8.49-8.52 (m, 2H), 7.72 (t, *J* = 8.0, 1H), 7.26 (d, *J* = 8.0, 1H), 4.18 (t, *J* = 7.4, 2H), 3.74 (t, *J* = 7.0 Hz, 2H), 3.59 (t, *J* = 7.0 Hz, 2H), 3.10 (s, 3H), 1.71 (m, 2H), 1.45 (m, 2H), 0.98 (t, *J* = 7.4 Hz, 3H). HRMS (ESI) calcd for $C_{19}H_{22}BrN_2O_2$ [MH^+] 389.0865, found 389.0862.

Synthesis of 3. Compound **7** (1.94 g, 5 mmol), aniline (0.548 mL, 6 Mmol), and triethylamine (0.836 mL, 6 mmol) were dissolved in 20 mL 2-methoxyethanol under nitrogen atmosphere. The solution was heated to reflux for 24 h and monitored by TLC. After cooling to room temperature, the mixture was added to 50 mL ice water. The product was filtered and further purified by column chromatography (SiO_2, PE:EA = 2:1, v/v) to give **3** as orange solid in 59.8% yield (1.2 g). ^{1}H NMR (400 MHz, $CDCl_3$) δ 8.56 (d, *J* = 7.8 Hz, 1H), 8.48 – 8.51 (m, 2H), 7.61 (t, *J* = 7.8 Hz, 1H), 7.26 (d, *J* = 7.8 Hz, 1H), 7.16 (t, *J* = 7.8 Hz, 2H), 6.72 (t, *J* = 7.4 Hz, 1H), 6.60 (d, *J* = 7.8 Hz, 2H), 4.17 (t, *J* = 7.6 Hz, 2H), 3.57 (t, *J* = 6.0 Hz, 2H), 3.48 (t, *J* = 6.0 Hz, 2H), 3.07 (s, 3H), 1.70 (m, 2H), 1.45 (m, 2H), 0.97 (t, *J* = 7.4 Hz, 3H). HRMS (ESI) calcd for $C_{25}H_{28}N_3O_2$ [MH^+] 402.2182, found 402.2180.

Synthesis of 1. Compound **2** (0.40 g, 1 mmol), K_2CO_3 (0.28 g, 2 mmol), KI (0.33 g, 2 mmol), 9-chloromethylanthracene (0.45 g, 2 mmol) were added to 20 mL 2-methoxyethanol. The solution was heated to reflux for 8 h and monitored by TLC. After cooling to room temperature, the solution was poured into 50 mL ice water. The product was filtered and further purified by column chromatography (SiO_2, PE:EA = 2:1, v/v) to give **1** a yellow solid in 61.1% yield (0.36 g). ^{1}H NMR (400 MHz, $CDCl_3$) δ 8.47 (d, *J* = 7.6 Hz, 1H), 8.32 (s, 1H), 8.10 (d, *J* = 8.0 Hz, 2H), 8.03 (d, *J* = 8.0 Hz, 1H), 7.94 (d, *J* = 8.0 Hz, 2H), 7.88 (d, *J* = 8.0 Hz, 1H), 7.49 – 7.32 (m, 7H), 7.04 (d, *J* = 8.2 Hz, 2H), 6.89 (t, *J* = 7.2 Hz, 1H), 6.41 (d, *J* = 8.0 Hz, 1H), 5.25 (s, 2H), 4.19 (t, *J* = 7.6 Hz, 2H), 3.30 (t, *J* = 7.6 Hz, 2H), 3.05 (t, *J* = 7.6 Hz, 2H), 2.48 (s, 3H), 1.76 (m, 2H), 1.49 (m, 2H), 1.00 (t, *J* = 7.4 Hz, 3H). ^{13}C NMR (100 MHz, $CDCl_3$) δ 164.62, 163.93, 155.10, 149.31, 131.78, 131.32, 131.13, 130.78, 130.07, 129.64, 129.20, 128.39, 127.42, 126.56, 125.41, 125.06, 124.87, 123.97, 122.95, 117.87, 115.51, 114.62, 113.14, 54.50, 45.94, 44.79, 41.13, 40.05, 30.35, 20.48, 13.89. HRMS (ESI) calcd for $C_{40}H_{38}N_3O_2$ [MH^+] 592.2964, found 592.2967.

Synthesis of 2. 0.2 mL Acetic acid was added to a solution of aniline (1.1 mL, 0.012 mol) in 20 mL dry toluene. Then a solution of 9-Anthraldehyde (2.06 g, 0.01 mol) in10 mL toluene was dropwise added. The mixture was heated to reflux for 3 h, and then the solvent was removed under reduced pressure. The residue was dissolved in 50 mL ethanol/DMF (3:2, v/v) solution,

followed by the addition of 0.757 g sodium tetrahydridoborate (0.02 mol) in portions. After being heated at 100˚C for 3h, the mixture was diluted with 100 mL of water, and treated with dilute acetic acid to decompose excess $NaBH_4$. The precipitate was filtered off, washed with water, and dried in air. The product was purified by column chromatography (SiO_2, PE:EA = 5:1, v/v) to give **2** faint yellow solid in 80.5% yield (2.28 g). ^{1}H NMR (400 MHz, $CDCl_3$) δ 8.47 (s, 1H), 8.27 (d, *J* = 8.2 Hz, 2H), 8.03 (d, *J* = 7.6 Hz, 2H), 7.46 – 7.53 (m, 4H), 7.29 (t, *J* = 8.0 Hz, 2H), 6.81 – 6.83 (m, 3H), 5.16 (s, 2H). HRMS (ESI) calcd for $C_{21}H_{18}N$ [MH^+] 284.1439, found 284.1436.

Synthesis of 4. 4-Bromo-1,8-naphthalic anhydride (1 g, 3 mmol) and 10 mL *N*-Methylpropylamine were dissolved in 20 mL ethanol. The mixture was refluxed for 24 h. After cooling to room temperature, the product was filtered to give 0.71 g as a yellow powder in 72.9% yield without further purification. ^{1}H NMR (400 MHz, $CDCl_3$) δ 8.58 (d, *J* = 8.0, 1H), 8.48 (d, *J* = 8.0 Hz, 1H), 8.44 (d, *J* = 8.0 Hz, 1H), 7.66 (t, J = 8.0, 1H), 7.17 (d, *J* = 8.0 Hz, 1H), 4.17 (t, *J* = 7.6 Hz, 2H), 3.32 (t, *J* = 7.2 Hz, 2H), 3.05 (s, 3H), 1.78 – 1.64 (m, 4H), 1.46 (m, 2H), 1.40 (m, 2H), 0.95 (t, *J* = 7.6, 3H), 0.92 (t, *J* = 7.2, 3H). HRMS (EI) calcd for $C_{21}H_{26}N_2O_2$ [M^+] 338.1994, found 338.1995.

Single Crystal X-ray Crystallographic Analysis

Crystals were obtained by direct diffusion of ether into a solution of sensor **1** in dichloromethane. A suitable single crystal was mounted in a glass fiber, and X-ray photoelectron spectroscopy (XPS) was performed with a Thermo VG ESCALABMK2 system operating in the parallel data acquisition mode using monochromatic Al Kα radiation ($h\nu$ = 1486.68 eV; spot size 400 μm). The refinement and all further calculations were carried out using SHELXL-97. The non-H atoms were refined anisotropically, using weighted full-matrix least-squares on F^2. Absorption correction were applied based on multiple and symmetry-equivalent measurements. The hydrogen atoms were included in the models in calculated positions and were refined as constrained to bonding atoms.

It is interesting to note that naphthalene ring and anthracene ring have a face-to-face alignment, due to strong π-π stacking interactions (Figure S3). The angle between naphthalene ring and anthracene ring is 19.9 °, owing to steric hindrance effects. The distances between naphthalene ring (C25-C36) and anthracene ring centroids (C1-C14) is ~3.98 Å, within the effective distance of 10—100 Å required for FRET[1]. The centroid distance between the anthracene rings of two neighboring molecules amounts to 5.04 Å, with a vertical separation of 3.58 Å (Figure S3).

Fluorescent Quantum Yields

Fluorescent quantum yields were determined using quinine sulfate as a reference. For sensor **1** and quinine sulfate, the absorbance spectra were measured within an absorbance range of 0.02 to 0.08. The quantum yield was calculated with the expression in Equation 1:

$$\Phi_{sample} = \Phi_{standard} \times \frac{\int emission_{sample}}{\int emission_{standard}} \qquad \text{Equation 1}$$

where $\Phi_{standard} = \Phi_{(quinine\ sulfate)} = 0.55$ in 0.1 M H_2SO_4.

Correlations between Fluorescence Intensity/Lifetime and Solvent Viscosity

The relationship between solvent viscosity (η) and dye fluorescence intensity (I) is described by the Förster-Hoffmann equation (Equation 2)[2]:

$$\log I = C + x \log \eta \qquad \text{Equation 2}$$

where C is a temperature- and concentration-dependent constant and x is a dye-dependent constant. Our results matched well with the Förster–Hoffmann equation. As shown in Figure 2a, R^2 of the linear relationship was as high as 0.984 , with a slope of x = 0.771. The R^2 and x in the inset of Figure 2b were 0.99 and 0.22, respectively.

The relationship between solvent viscosity (η) and dye fluorescence lifetime (τ_f) is summarized in Equations 3 and 4[2]:

$$\log \tau_f = C + x \log \eta \qquad \text{Equation 3}$$

$$\tau = z\, k_0\, \eta^{\alpha} \qquad \text{Equation 4}$$

where C is a temperature- and concentration-dependent constant and x is a dye-dependent constant; k_0 is the radiative rate constant, and z and α are constants. As shown in Figure 2d, a good relationship between $\log \tau_f$ and $\log \eta$ ($R^2 = 0.987$, x = 0.13) was obtained in our results.

Computational Methods

In order to understand the energetic stability of these different conformations and their impact on the optoelectronic properties of **1**, quantum mechanical calculations were performed on **1** using *Gaussian 09*[3], with a special interest on the relative alignment between N_1 and N_2, *i.e.*, the N-shaped and U-shaped alignments. These calculations were executed via six steps:

- Step 1: generated conformers of **1** using Confab (RMSD cutoff threshold: 0.5 Å; energy cutoff threshold: 10 kcal/mol)[4]. 104 conformers of **1** were thereof found.
- Step 2: optimized the molecular geometries of the resulting conformers using the PM6 method in the gas phase[5]. In order to reduce the computational load, the butyl group in the 1, 8-naphthalimide fluorophore was replaced by a methyl group in this step. This replacement is reasonable, because the butyl/methyl groups do not affect the properties of **1** much.

- Step 3: 12 most stable conformers of **1**, which includes both the N-shaped and U-shaped alignments, were selected and sent for further geometry optimizations in the gas phase, via density functional theory (DFT) based calculations. Becke's three-parameter and Lee-Yang-Parr hybrid functional (B3LYP)[6-8] and a 3-21G basis set[9-11] were used. The butyl group, previously replaced by a methyl group, was restored from this step onwards.
- Step 4: six most stable conformers of **1** from the previous cycle were selected for further geometry optimizations using the B3LYP functional and a 6-31G(d) basis set[12], in ethylene glycol solution, as accounted for via the polarizable continuum model (PCM) [13,14]. These optimizations were followed by single point calculations using B3LYP/6-31+G(d,p) in order to accurately determine the relative energetic stability of all six conformers.
- Step 5: time-dependent DFT (TD-DFT) calculations were performed on the most stable N-shaped and U-shaped conformers of **1**.

In particular, the crystal structure of **1** had been determined in-house, with the N-shaped alignment between its N_1 and N_2. Using its molecular structure in the crystal environment as a starting point, we have optimized the geometry of **1** and performed TD-DFT calculations on the resulting molecular structure as well.

In all calculations, frequency checks were performed after each geometry optimization in order to ensure that minima on the potential energy surfaces were found.

Experimental Results

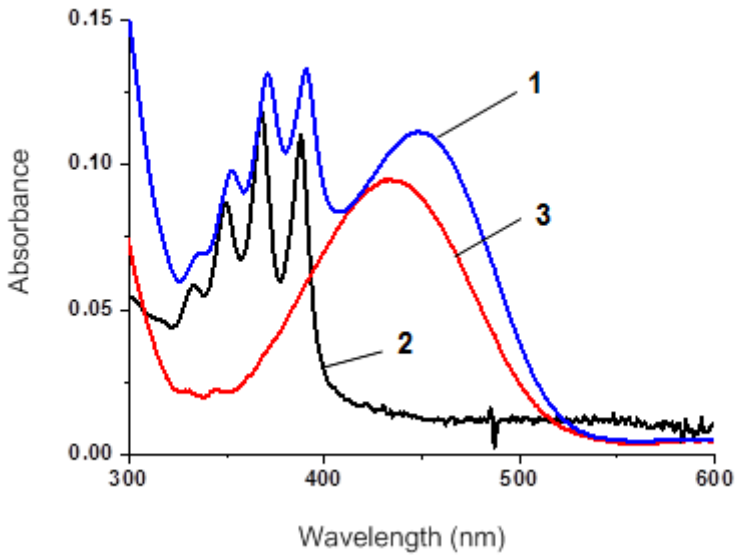

Figure S1. The UV-Vis absorption spectra of compounds **1**—**3** (10 μM) in ethylene glycol.

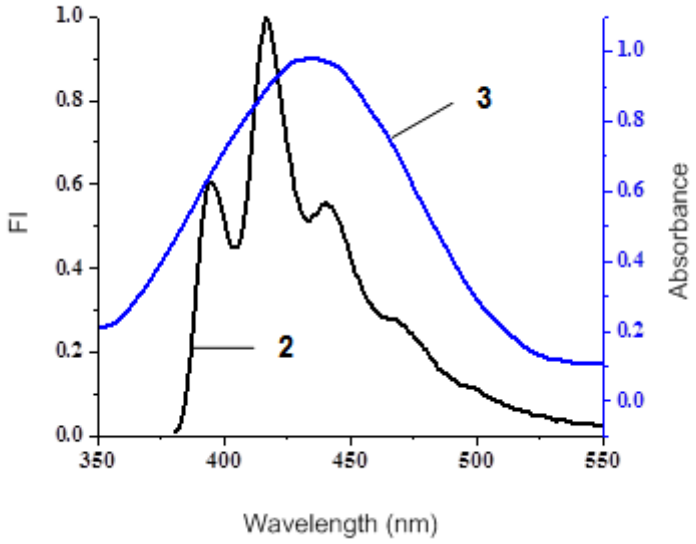

Figure S2. The spectral overlap between the emission of **2** and the absorption of **3** in ethylene glycol.

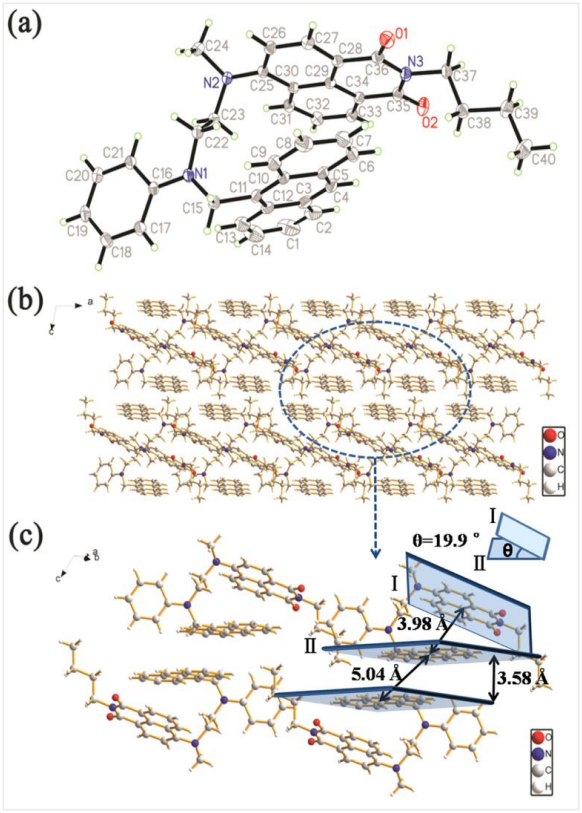

Figure S3. (a) Crystal structures of **1** with displacement ellipsoids showing at the 50% probability level in a unit cell; (b) crystal packing diagrams viewed along the c-axis; (c) partially enlarged display.

Table S1. Crystal data and structure refinement summary for **1**

Compound	**1**
Formula	$C_{40}H_{37}N_3O_2$
Fw	591.73
Crystal system, space group	Triclinic，P-1
a (Å)	10.3004(2)
b (Å)	12.8375(3)
c (Å)	13.6157(4)
α (°)	116.810(2)
β (°)	94.392(2)
γ (°)	102.800(2)
V (Å^3)	1534.39(6)
Z, Calculated density (Mg/m^3)	2, 1.281
Absorption coefficient/mm^{-1}	0.079
Data / restraints / parameters	5374 / 0 / 407
F (000)	628
Crystal size/mm	0.08×0.03×0.02
Limiting indices	-12<=h<=12,–14≤*k*≤15, –16≤*l*≤7
Reflections collected/unique	9112/5374 [*R(int)* = 0.0250]

Goodness–of–fit on F^2	1.004
Final R indices [I>2sigma(I)]	R_1 = 0.0482, wR_2 = 0.1231
R indices (all data)	R_1 = 0.0758, wR_2 = 0.1369
Largest diff. peak and hole（e.Å^{-3}）	0.228 and -0.212

Table S2. Selected bond lengths (Å) and angles (°) for **1**

Compound		Bond lengths		Bond angles
1	C(11)-C(15)	1.519(3)	C(16)-N(1)-C(22)	120.17(15)
	N(1)-C(15)	1.464(2)	C(16)-N(1)-C(15)	121.84(14)
	N(1)-C(22)	1.457(2)	C(22)-N(1)-C(15)	116.54(15)
	C(22)-C(23)	1.533(2)	C(25)-N(2)-C(24)	116.89(15)
	N(2)-C(24)	1.461(2)	C(25)-N(2)-C(23)	115.25(14)
	N(2)-C(23)	1.473(2)	C(24)-N(2)-C(23)	113.50(15)
	N(2)-C(25)	1.403(2)	C(35)-N(3)-C(36)	124.36(16)
	N(3)-C(35)	1.398(2)	N(1)-C(22)-C(23)	112.38(15)
	N(3)-C(36)	1.400(2)	N(2)-C(23)-C(22)	113.82(15)
	N(3)-C(37)	1.473(2)	N(1)-C(15)-C(11)	112.76(14)
	O(1)-C(36)	1.224(2)	O(1)-C(36)-N(3)	119.96(18)
	O(2)-C(35)	1.219(2)	O(2)-C(35)-N(3)	120.00(18)

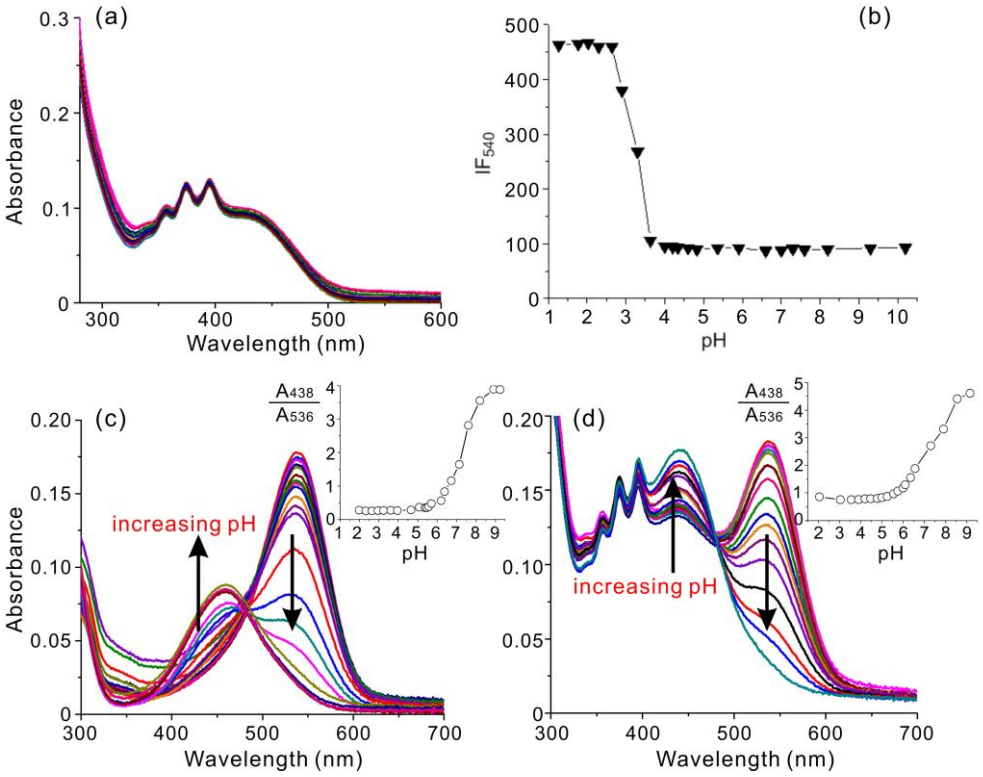

Figure S4. (a) The UV-Vis absorption spectra of **1** in aqueous solutions (DMSO/H_2O = 10:90, v/v; [**1**] = 10 μM) of various pH values from 2 to 9; (b) the influence of pH on the fluorescence intensity of **1** at 540 nm in aqueous solutions, excited at 430 nm ([**1**] = 10 μM); the UV-Vis

absorption spectra of (c) **NR** and (d) a mixture of **1** and **NR** in aqueous solutions of various pH values from 2 to 9 ([**1**] = [**NR**] = 10 μM). The insets in (c) and (d) show the relative values between the absorbance at 438 and 536 nm. The UV—Vis absorption and emission profiles of **1** exhibit little pH dependence, in contrast to that of **NR**.

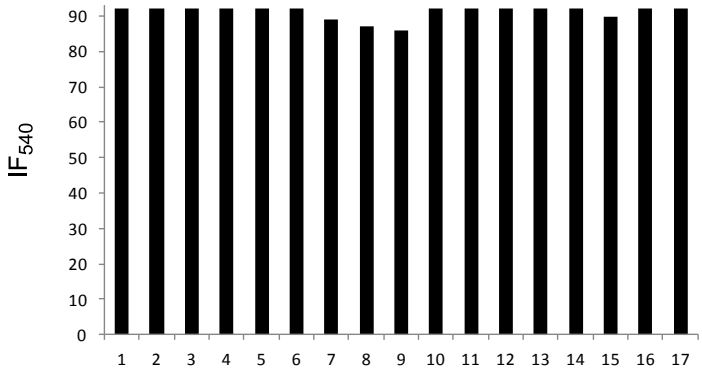

Figure S5. Fluorescence responses of 10 μM **1** to various metal ions in aqueous solution (DMSO: 0.5 M HEPES (pH 7.4) = 10:90, v/v), excited at 430 nm. 1) Free **1**; 2) Li^{+}; 3) Na^{+}; 4) K^{+}; 5) Mg^{2+}; 6) Ca^{2+}; 7) Co^{2+}; 8) Ni^{2+}; 9) Cu^{2+}; 10) Zn^{2+}; 11) Cd^{2+}; 12) Fe^{2+}; 13) Fe^{3+}; 14) Cr^{3+}; 15) Ag^{+}; 16) Hg^{2+}; 17) Pb^{2+}.

Table S3. The absorption, emission and quantum yield information of **1** in different solvents.[a]

Solvents	λ_{ab} (nm)				λ_{em} (nm)[1]				Φ
DCM	351	370	390	420	392	413	439	502	0.012349
Toluene	352	370	390	421	504				0.13904
THF	351	369	389	415	390	430	520		0.006903
Acetone	350	368	388	420	391	417	440	508	0.005277
DMF	352	370	390	427	408	432	457		0.058725
Ethanol	350	368	388	434	390	414	458		0.00365
Methanol	350	368	387	435	390	413	463		0.002334
DMSO	353	371	392	432	391	415	450		0.004519
Water	355	370	391	435	390	423	453		0.004249
Ethylene Glycol	352	370	391	447	390	405	440		0.010741
Glycerol	357	374	395	450	394	419	440	540	0.365194

[a] Excitation wavelength = 370 nm.

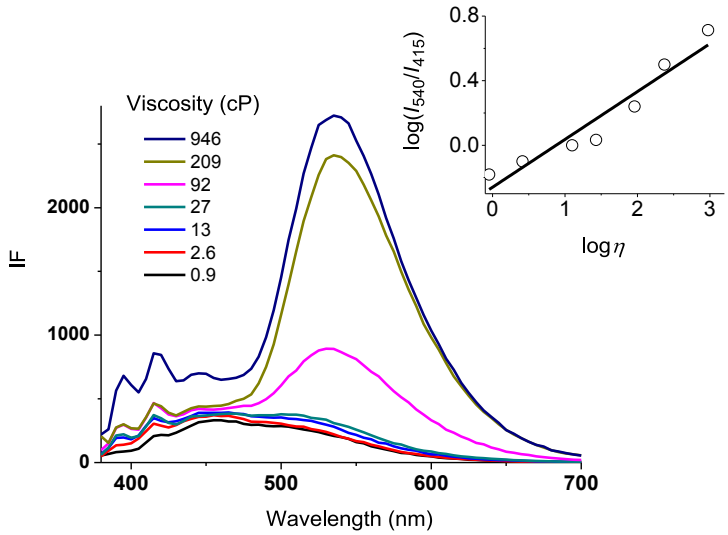

Figure S6. Fluorescent spectra of 10 μM **1** in water-glycerol mixtures with varied viscosity, excited at 370 nm. Inset: the linearity between $\log(I_{540}/I_{415})$ and $\log\eta$.

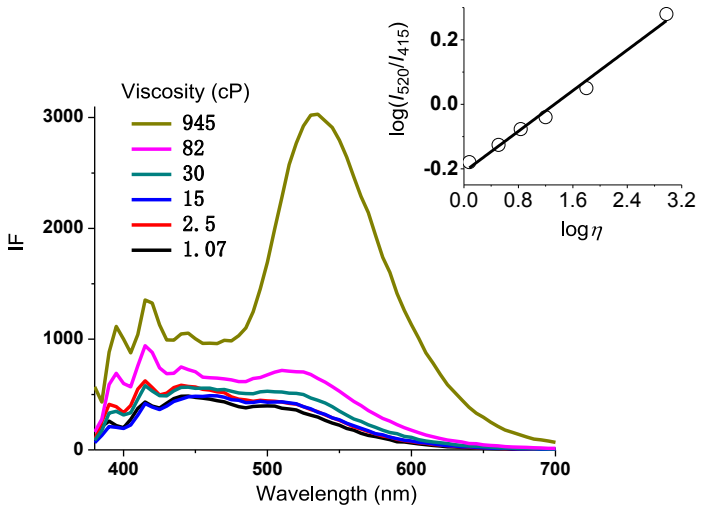

Figure S7. Fluorescent spectra of 10 μM **1** in ethanol-glycerol mixtures with varied viscosity, excited at 370 nm. Inset: the linearity between $\log(I_{520}/I_{415})$ and $\log\eta$.

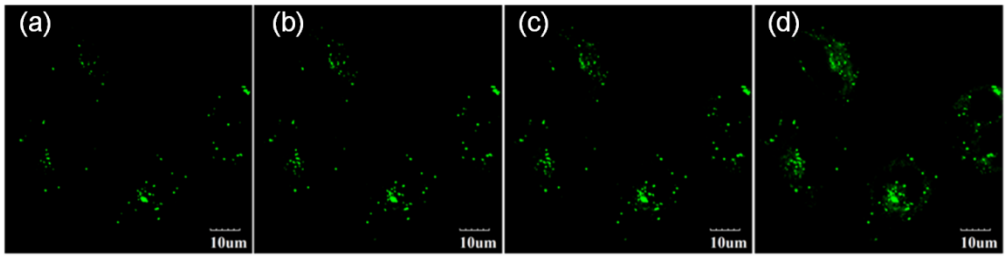

Figure S8. Time-dependent fluorescence changes of MCF-7 cells stained with **1** for: (a) 0.5 min; (b) 1 min; (c) 2 min; (d) 3 min. Excitation wavelength = 405 nm; emission wavelength = 530—570 nm.

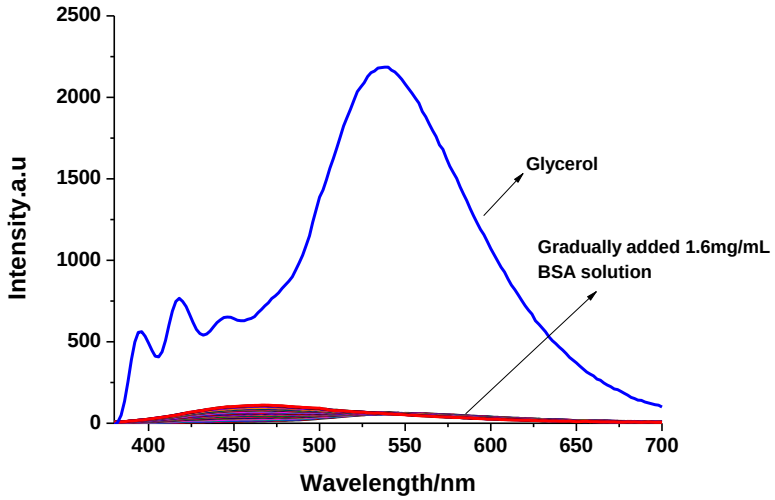

Figure S9. Fluorescence properties of **1** in the presence of BSA (Albumin from bovine serum).

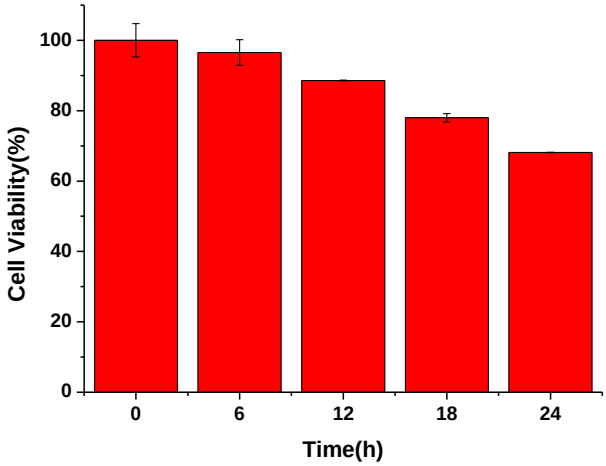

Figure S10. Cytotoxicity studies of sensor **1** (5 μmol) in MCF-7 cells.

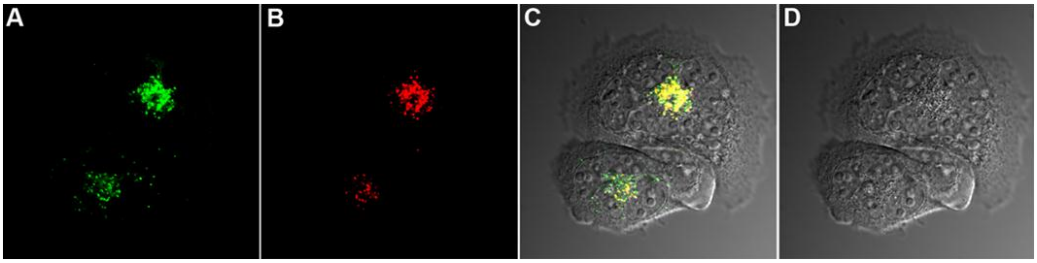

Figure S11. Fluorescent images of a SMMC 7721 cell co-incubated with 3 μM **1** and 3 μM neutral red (**NR**) for 3 min at 37 ℃. (a) Fluorescent confocal image from **1** (Channel 1: λex = 405 nm, λem = 530—570 nm); (b) fluorescent confocal image from **NR** (Channel 2: λex = 559 nm, λem = 570—610 nm); (c) the merged image of channels 1 and 2; (d) bright-field image.

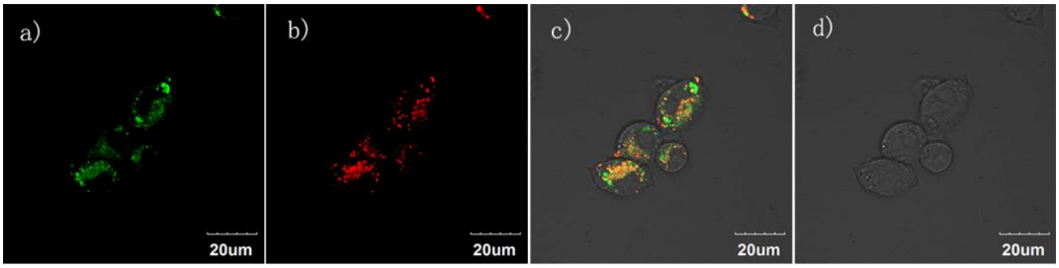

Figure S12. Fluorescent images of BV2 co-incubated with 3 μM **1** and 3μM **NR** for 3 min at 37 ℃. (a) Fluorescent confocal image from **1** (Channel 1: λex = 405 nm, λem = 530—570 nm); (b) fluorescent confocal image from **NR** (Channel 2: λex = 559 nm, λem = 570—610 nm); (c) the merged image of channels 1 and 2; (d) bright-field image.

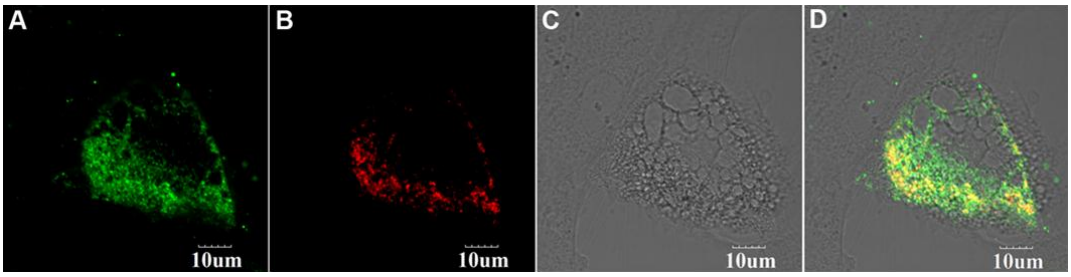

Figure S13. Fluorescent images of a cardiac muscle cell co-incubated with 3 μM **1** and 3 μM **NR** for 3 min at 37 ℃. (a) Fluorescent confocal image from **1** (Channel 1: λex = 405 nm, λem = 530—570 nm); (b) fluorescent confocal image from **NR** (Channel 2: λex = 559 nm, λem = 570—610 nm); (c) bright-field image; (d) the merged image of channels 1 and 2.

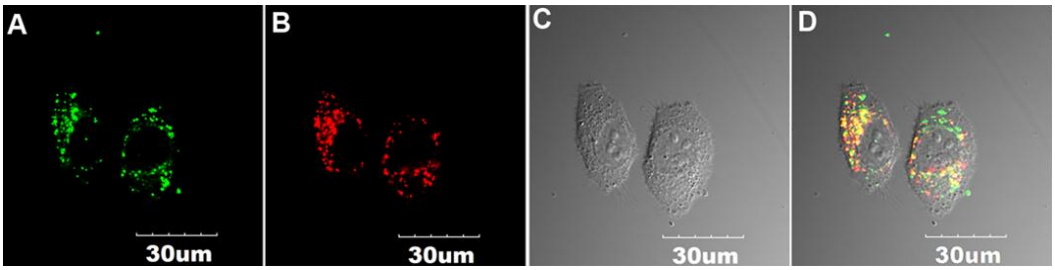

Figure S14. Fluorescent images of Hela co-incubated with 3 μM **1** and 3 μM **NR** for 3 min at 37 ℃. (a) Fluorescent confocal image from **1** (Channel 1: λex = 405 nm, λem = 530—570 nm); (b) fluorescent confocal image from **NR** (Channel 2: λex = 559 nm, λem = 570—610 nm); (c) bright-field image; (d) the merged image of channels 1 and 2.

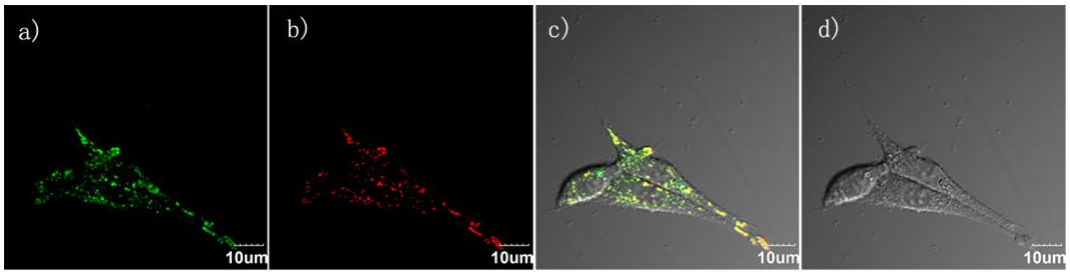

Figure S15. Fluorescent images of a PC12 cell co-incubated with 3 μM **1** and 3 μM **NR** for 3 min at 37 ℃. (a) Fluorescent confocal image from **1** (Channel 1: λex = 405 nm, λem = 530—570 nm); (b) fluorescent confocal image from **NR** (Channel 2: λex = 559 nm, λem = 570-610 nm); (c) the merged image of channels 1 and 2; (d) bright—field image.

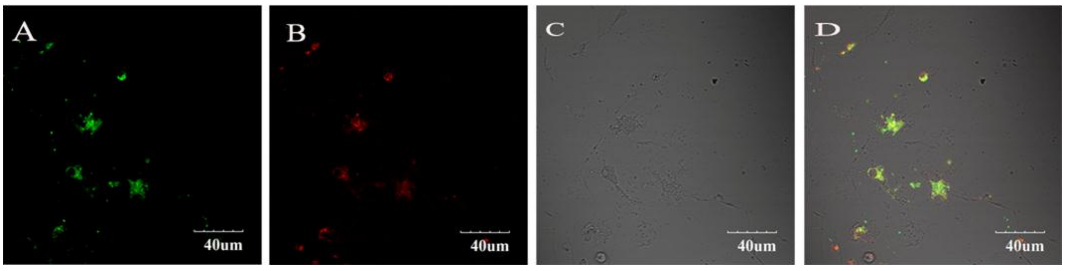

Figure S16. Fluorescent images of a neural stem cell co-incubated with 3 μM **1** and 3 μM **NR** for 3 min at 37 ℃. (a) Fluorescent confocal image from **1** (Channel 1: λex = 405 nm, λem = 530—570 nm); (b) fluorescent confocal image from **NR** (Channel 2: λex = 559 nm, λem = 570—610 nm); (c) bright-field image; (d) the merged image of channels 1 and 2.

Computational Results

The energies and optoelectronic properties of representative conformers of **1**, calculated via DFT/TD-DFT, are summarized in Table S4.

Table S4. Energetic stability of representative conformers of **1**, and their electronic excitation energy, oscillator strengths, configuration interactions of low-lying excited states in ethylene glycol.

compound/ conformation	relative energy (eV)[a]	electronic transition	energy	f^b	composition	CI
N-shaped conformer (extended form, without π-π interactions)	0	S0→S1	2.4562 eV (504.77 nm)	0.0013	HOMO→LUMO	0.7062
		S0→S2	2.7095 eV (457.58 nm)	0.0077	HOMO-1→LUMO	0.7058
		S0→S3	2.7613 eV (449.00 nm)	0.0002	HOMO→LUMO+1	0.7052

		S0→S4	2.9330 eV (422.72 nm)	**0.3733**	HOMO-2→LUMO	0.6959
		S0→S5	3.0976 eV (400.25 nm)	**0.1140**	HOMO-1→LUMO+1	0.6990
		S0→S6	3.4124 eV (363.34 nm)	0.0008	HOMO-2→LUMO+1	0.7050
N-shaped conformer (folded form, with strong π-π interactions)[c]	0.0083	S0→S1	2.4684 eV (502.29 nm)	**0.1066**	HOMO→ LUMO	0.7019
		S0→S2	2.5538 eV (485.50 nm)	0.0100	HOMO-1→LUMO	0.7049
		S0→S3	2.7319 eV (453.84 nm)	0.0016	HOMO→ LUMO+1	0.7045
		S0→S4	2.9702 eV (417.43 nm)	**0.1217**	HOMO-2 → LUMO	**0.6887**
					HOMO-1→LUMO+1	-0.1175
		S0→S5	3.1051 eV (399.29 nm)	**0.1636**	HOMO-2→LUMO	0.1173
					HOMO-1→LUMO+1	**0.6902**
		S0→S6	3.2900 eV (376.86 nm)	0.0026	HOMO-2 →LUMO+1	0.7061
U-shaped conformer	0.0604	S0→S1	2.4414 eV (507.84 nm)	**0.0336**	HOMO→ LUMO	0.7057
		S0→S2	2.6926 eV (460.47 nm)	0.0001	HOMO-1→LUMO	0.6721
					HOMO→ LUMO+1	0.2131
		S0→S3	2.6992 eV (459.34 nm)	0.0129	HOMO-1→LUMO	-0.2161
					HOMO-1→LUMO+1	0.1077
					HOMO→ LUMO+1	0.6622
		S0→S4	2.9513 eV (420.09 nm)	**0.3435**	HOMO-2→LUMO	0.6937
		S0→S5	3.1107 eV (398.57 nm)	**0.1276**	HOMO-1→LUMO+1	0.6863
					HOMO→ LUMO+1	-0.1116
		S0→S6	3.3470 eV (370.43 nm)	0.0003	HOMO-2 → LUMO+1	0.7048

[a] The single point energy of the most stable conformer is set to 0

[b] Oscillator strength. Major transitions (with f>0.02) are highlighted in bold.

[c] This conformer of **1** was geometrically optimized based on its molecular structure determined via single crystal XRD.

The atomic coordinates of the representative N-shaped and U-shaped conformers of **1** are listed in Tables S5-7.

Table S5. Atomic coordinates of the N-shaped conformer of **1** (extended form without π-π stacking interactions)

C -3.65451900 2.11428800 1.23804400

C	-2.28755800	2.11419500	1.56368700
C	-1.48678200	1.04382200	1.20767200
C	-2.00963600	-0.06908600	0.50415900
C	-3.41485200	-0.09623700	0.24434500
C	-4.21652300	1.01969400	0.59977000
C	-1.19897400	-1.19804900	0.10711500
C	-1.84361200	-2.33193700	-0.39190600
C	-3.22824300	-2.35190400	-0.60544500
C	-4.01707400	-1.24654600	-0.32609700
C	-5.46160400	-1.28461000	-0.60124000
N	-6.19764300	-0.12579700	-0.29749100
C	-5.66942400	1.01753100	0.31280500
O	-6.39828700	1.96897100	0.58930700
O	-6.02806500	-2.26681300	-1.07985800
N	0.19336400	-1.14724400	0.27164200
C	0.92938300	-0.12409800	-0.50392800
C	0.89600000	-2.42979000	0.31946000
C	2.10179600	0.50271300	0.27911400
N	2.94803400	1.37258000	-0.53360700
C	2.43500700	2.57172500	-1.04329400
C	1.34473100	3.22524400	-0.42036700
C	0.86226400	4.44051600	-0.89854500
C	1.43674800	5.05871100	-2.01225000
C	2.50547000	4.42225100	-2.64258100
C	2.99630000	3.20054700	-2.17940200
C	4.14956500	0.80727200	-1.17419300
C	4.87884500	-0.24371600	-0.35454800
C	4.90323700	-1.60293000	-0.75614400
C	5.67525900	-2.55889000	0.01374000
C	6.37682600	-2.13147300	1.14371800
C	6.35389100	-0.79668400	1.55922200
C	5.59161600	0.16793600	0.80029400
C	7.07676200	-0.37022300	2.71768700
C	7.05679500	0.93879600	3.11950900
C	6.30598300	1.89567500	2.37864000
C	5.59857100	1.52534400	1.26276700
C	4.19670900	-2.11071800	-1.89899600
C	4.25305900	-3.43498100	-2.25127000
C	5.02146200	-4.36324000	-1.49201500
C	5.70998000	-3.93140900	-0.39116000
H	-4.29127000	2.95108600	1.50416200
H	-1.86295800	2.94967000	2.11148600
H	-0.44562600	1.03162600	1.50673500
H	-1.26640300	-3.20382000	-0.67377000

H	-3.69638400	-3.23435500	-1.02938400
H	0.23189400	0.65565200	-0.81330200
H	1.31732200	-0.58492600	-1.42616200
H	0.38407600	-3.10781300	1.00613200
H	1.90873200	-2.26921700	0.69507500
H	0.97762300	-2.91176300	-0.66740300
H	2.74080500	-0.28175300	0.68509900
H	1.72148900	1.05314500	1.14636100
H	0.87239500	2.79191100	0.45263600
H	0.02473300	4.90773800	-0.38626100
H	1.05604600	6.00651500	-2.38107100
H	2.96659900	4.87028000	-3.51948800
H	3.80776300	2.73536900	-2.72490400
H	4.84594000	1.63765000	-1.33095700
H	3.92087800	0.42480700	-2.17527600
H	6.95451200	-2.85547700	1.71426200
H	7.64412700	-1.11338000	3.27250500
H	7.60913100	1.25280500	4.00062600
H	6.29226900	2.93178400	2.70559200
H	5.01848700	2.27081600	0.73198600
H	3.59634900	-1.44176300	-2.50420100
H	3.70411200	-3.78216200	-3.12221900
H	5.05479400	-5.40722900	-1.78996500
H	6.29953400	-4.62549400	0.20272700
C	-7.64209400	-0.13598000	-0.59533200
C	-8.48655300	-0.66106800	0.57079900
H	-7.77816600	-0.76270300	-1.47751100
H	-7.92308800	0.88948900	-0.83923400
C	-9.98494900	-0.66215200	0.24273600
H	-8.16001300	-1.67931800	0.81795300
H	-8.30141500	-0.03854900	1.45544100
C	-10.84642200	-1.18159300	1.39834600
H	-10.30015200	0.35750500	-0.01980800
H	-10.16091100	-1.27741900	-0.65078600
H	-11.91062900	-1.17169700	1.13675600
H	-10.57594900	-2.21167300	1.66098900
H	-10.71677000	-0.56503400	2.29627000

Table S6. Atomic coordinates of the N-shaped conformer of **1** (folded form with strong π-π stacking interactions; optimized based on the molecular structure determined via XRD)

O	-4.43780900	2.06951600	1.78736300
O	-4.83497000	0.02532800	-2.28015600
N	3.92383600	-0.18968300	0.56239500

N	1.63445400	2.75026100	-0.29254600
N	-4.63758200	1.06650800	-0.25717200
C	1.12703700	-2.70722300	-3.62146600
H	0.92618500	-2.94736800	-4.66165400
C	0.12233400	-2.75166100	-2.69193600
H	-0.88948800	-3.02553400	-2.98012400
C	0.37346600	-2.43949300	-1.31859000
C	-0.65162400	-2.48453800	-0.36901000
H	-1.65644600	-2.75627600	-0.68492300
C	-0.41691500	-2.18916200	0.97624500
C	-1.48201200	-2.23441000	1.93131100
H	-2.47504400	-2.50218600	1.57879100
C	-1.26272100	-1.94700400	3.25128600
H	-2.07866200	-1.98368400	3.96730800
C	0.04619200	-1.59423400	3.68770600
H	0.21518900	-1.36133600	4.73538800
C	1.09434200	-1.54305900	2.80478000
H	2.07202800	-1.26216900	3.17855600
C	0.92052900	-1.83794900	1.40988400
C	1.97331800	-1.79548100	0.46167200
C	1.70962900	-2.07916000	-0.90248700
C	2.72512500	-2.03468700	-1.91511900
H	3.73195000	-1.73576500	-1.64779500
C	2.44370200	-2.33864300	-3.22328400
H	3.23385900	-2.29548200	-3.96786300
C	3.40690300	-1.53060100	0.89083200
H	4.03839600	-2.25590000	0.37223100
H	3.52983400	-1.74363300	1.96013500
C	5.31193200	0.00562500	0.61853900
C	6.20565300	-1.03344400	0.96642000
H	5.83582100	-2.01092000	1.24921100
C	7.58507900	-0.82104700	0.98259800
H	8.23641700	-1.64707000	1.25781600
C	8.12916700	0.42469300	0.67116100
H	9.20329600	0.58375700	0.68865700
C	7.25673000	1.46411900	0.33864300
H	7.64892600	2.44717100	0.08969300
C	5.87890500	1.26495800	0.30899700
H	5.24315500	2.09464100	0.02322500
C	3.04206100	0.95905100	0.79685800
H	2.18265800	0.63458700	1.38927600
H	3.57417200	1.70260700	1.39870800
C	2.51826200	1.59157500	-0.51457200
H	1.97844900	0.82444700	-1.06771800

H	3.35755000	1.91418100	-1.14141900
C	2.27133900	3.87888500	0.38403400
H	1.64903700	4.77022600	0.26912500
H	2.45354600	3.72137300	1.45679800
H	3.23560100	4.06816900	-0.09832000
C	0.27114800	2.53960100	-0.07023400
C	-0.36110000	2.99702400	1.08937500
H	0.21538000	3.51147600	1.84915800
C	-1.71565500	2.74105400	1.33288000
H	-2.16926400	3.06847000	2.26273500
C	-2.49067800	2.03550600	0.42380100
C	-1.91050000	1.62149100	-0.80270000
C	-0.53683600	1.89862100	-1.08505100
C	-0.05335500	1.60612500	-2.38508500
H	0.95415900	1.90273700	-2.65291000
C	-0.85563100	0.99219100	-3.33027100
H	-0.46340700	0.78570900	-4.32098200
C	-2.18096100	0.64592600	-3.01761400
H	-2.81543500	0.15236600	-3.74587600
C	-2.70915600	0.96792900	-1.77710000
C	-4.12339100	0.63999000	-1.48663900
C	-3.89920800	1.74598200	0.72865800
C	-6.04845200	0.75579200	0.03835200
H	-6.42149400	1.55656100	0.67785100
H	-6.58477400	0.77721800	-0.91124300
C	-6.22403600	-0.60399400	0.72335900
H	-5.64922100	-0.60991200	1.65837700
H	-5.80108000	-1.38588200	0.07953200
C	-7.69650400	-0.91647500	1.01851700
H	-8.11779600	-0.12041100	1.64836800
H	-8.26670300	-0.89871000	0.07919600
C	-7.88994200	-2.27050700	1.70893500
H	-8.94946300	-2.46820500	1.90731200
H	-7.50726700	-3.08933700	1.08739100
H	-7.35784000	-2.30445300	2.66749600

Table S7. Atomic coordinates of the U-shaped conformer of **1**

C	2.91984600	-2.04374300	-1.21036800
C	1.52111900	-1.93763600	-1.15039500
C	0.93008200	-0.88225500	-0.47886000
C	1.70336000	0.12065700	0.15668800
C	3.12533600	-0.03976000	0.16023300
C	3.71378800	-1.11821200	-0.55117800
C	1.12021700	1.24991000	0.85145700

C	1.96841600	2.05900900	1.61533900
C	3.35392800	1.86337200	1.63061100
C	3.94932200	0.84992800	0.89525400
C	5.41157900	0.70254300	0.89776700
N	5.94445500	-0.36844500	0.15849600
C	5.18554200	-1.27815000	-0.58565300
O	5.73747300	-2.16893200	-1.23043200
O	6.16258600	1.46391000	1.50773500
N	-0.25772100	1.49136000	0.78691200
C	-0.86149000	1.69172800	-0.55289900
C	-0.80849500	2.40453900	1.79113600
C	-2.18762400	0.95302100	-0.81979900
N	-3.34907600	1.37702400	-0.04392200
C	-3.88428000	2.65720600	-0.20659200
C	-3.61482900	3.42551000	-1.36486200
C	-4.17162500	4.69132900	-1.53335300
C	-5.01151400	5.24759500	-0.56536800
C	-5.27424200	4.50766900	0.58798800
C	-4.71818200	3.24212900	0.77602200
C	-3.92331300	0.46328900	0.95871400
C	-3.96021100	-1.00062200	0.54214800
C	-3.11339500	-1.95910900	1.15283500
C	-3.24159100	-3.35731400	0.79208700
C	-4.18239800	-3.73951100	-0.16703600
C	-5.00890300	-2.80355000	-0.79650400
C	-4.90011600	-1.40754000	-0.43896900
C	-5.96571800	-3.20817000	-1.78000700
C	-6.78158900	-2.29275200	-2.38963400
C	-6.68138900	-0.91514300	-2.04358800
C	-5.77544700	-0.48777800	-1.10565700
C	-2.10651300	-1.62815200	2.12223200
C	-1.31634100	-2.59104000	2.69623700
C	-1.46606200	-3.96453600	2.35008600
C	-2.40095900	-4.33070200	1.42032700
H	3.39604100	-2.85941000	-1.74365600
H	0.90050900	-2.69375900	-1.62085300
H	-0.14826000	-0.84412000	-0.40405900
H	1.56626500	2.89683100	2.16962300
H	3.98620800	2.53583000	2.20120900
H	-0.14816300	1.36066600	-1.31035900
H	-1.00048300	2.77118400	-0.70721100
H	-0.48515400	2.10151100	2.78987300
H	-1.89595300	2.35616600	1.74868900
H	-0.51104000	3.45149700	1.62144000

H	-2.05363400	-0.11292200	-0.63558600
H	-2.39339200	1.04524800	-1.89546900
H	-2.98035800	3.03084900	-2.14960600
H	-3.94577200	5.24478300	-2.44160900
H	-5.44176100	6.23505300	-0.70354400
H	-5.91007900	4.91993900	1.36767600
H	-4.91824200	2.72298500	1.70616900
H	-4.95610200	0.77846900	1.12555500
H	-3.42520700	0.56978200	1.92863300
H	-4.27282900	-4.79079900	-0.43171700
H	-6.02966300	-4.26397500	-2.03158300
H	-7.50506200	-2.60982400	-3.13533700
H	-7.33065300	-0.19382400	-2.53224000
H	-5.71626400	0.56963100	-0.87696900
H	-1.94506200	-0.59365100	2.39967300
H	-0.56190600	-2.30290300	3.42303700
H	-0.83300900	-4.71148800	2.82038900
H	-2.52301800	-5.37290700	1.13580300
C	7.41079600	-0.52410600	0.14005300
C	8.07375600	0.25166600	-1.00353900
H	7.61594700	-1.59140000	0.04708300
H	7.77882700	-0.17217400	1.10455700
C	9.59835600	0.08433700	-1.00837600
H	7.65919900	-0.09636500	-1.95840400
H	7.81795600	1.31493500	-0.90953600
C	10.27745900	0.85262800	-2.14679600
H	10.00422600	0.42307500	-0.04479600
H	9.84688300	-0.98335500	-1.08760600
H	11.36445800	0.71448200	-2.12670000
H	9.91488500	0.51260000	-3.12461400
H	10.07551800	1.92826200	-2.07344200

The DFT/TD-DFT Rationalization of Intramolecular PET in 1

The intramolecular PET process in **1** can be rationalized by considering the energy levels of the associated molecular orbitals (MOs) of both the electron donor and acceptor within this compound.

In some studies, the donor and acceptor are divided into two parts and the energy levels of their MOs are evaluated separately while investigating the thermodynamics of the intramolecular PET process[15,16]. However, this approach ignores the interactions between the donor and the acceptor, and the partition of the donor and the acceptor can be quite arbitrary[17]. Another approach is to compute the molecular orbitals of the entire molecule, and then separate its MOs into two parts, depending whether the electron distribution localizes in the donor or the acceptor region in

the molecule[17,18]. The second approach is used in this study.

In **1**, the 1, 8-naphthalimide fluorophore acts as an electron acceptor, while the aniline substituent at the 4-position functions as an electron donor during the PET process. TD-DFT calculations show that the first absorption bands of **1** mainly consist of HOMO-2 → LUMO transition for **1** (Figure S17); there are also minor contributions from HOMO → LUMO transitions. HOMO-2 and LUMO of **1** have very similar electron density distributions as compared to the HOMO and LUMO of 4-amino-1, 8-naphthalimide fluorophore (Figure S18). These two MOs are thus attributed to the PET acceptor. In contrast, the HOMO of **1** mainly localizes in the 4-position substituent of the fluorophore. Hence, it belongs to the PET donor. It is clear that this energy configuration allows the PET to occur in **1** from the thermodynamic point of view (Figure S19).

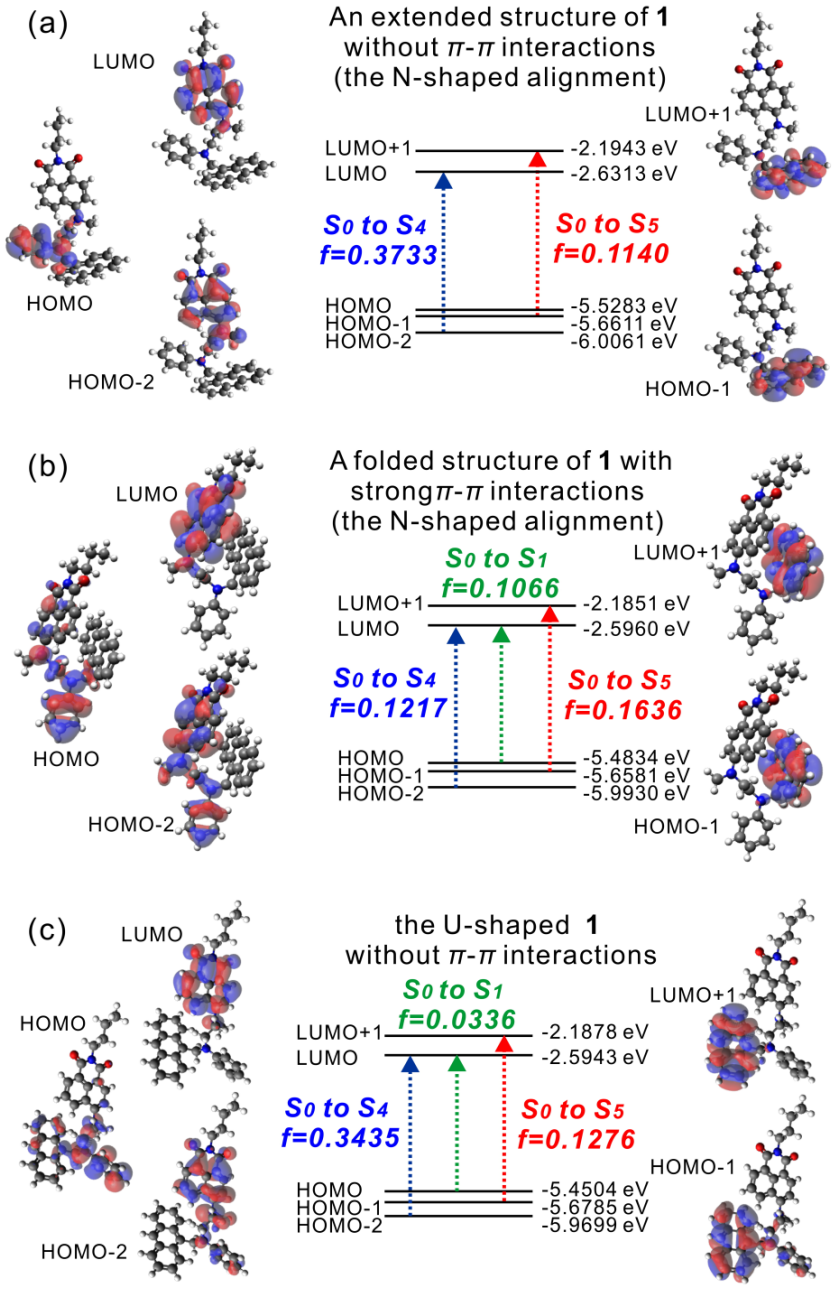

Figure S17. The frontier MOs and their energy levels of representative conformers of **1** (red:

positive; blue: negative; isovalue: 0.02).

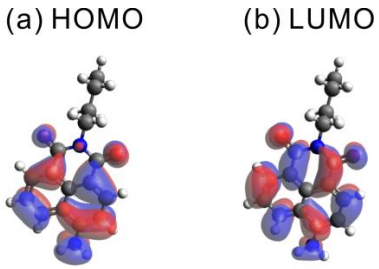

Figure S18. The HOMO and LUMO of 4-amino-1, 8-naphthalimide (red: positive; blue: negative; isovalue: 0.02).

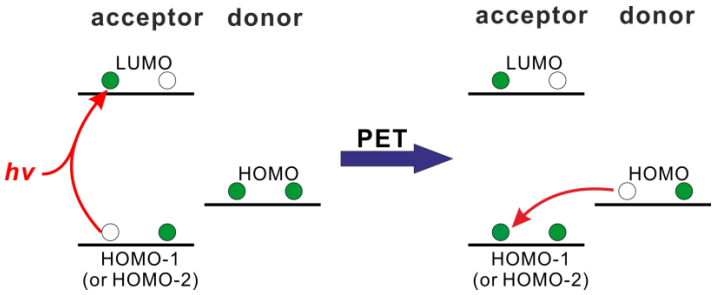

Figure S19. Schematic illustration of the energy levels of frontier MOs in **1** and the associated PET process.

Exponential Fittings to the Fluorescence Decay Kinetics of 1

The fluorescence lifetime of compounds **1** were measured in ethylene glycol and glycerol mixtures. The ratios of these two solvents were adjusted in order to produce mixtures of different viscosities, *i.e.*, 20.5, 28, 33, 116, 378, and 945 cP. The fluorescence decay kinetics was fitted to both a single-exponential function (Equation 5) and a double-exponential function (Equation 6). The associated fitting parameters and goodness-of-fit (reduced χ^2) were summarized in Table S8. The fluorescence decay curves and the best-fits are also plotted in Figure S20.

$$I(t) = A\exp\left(-\frac{t}{\tau}\right) + B \qquad \text{Equation 5}$$

$$I(t) = A_1\exp\left(-\frac{t}{\tau_1}\right) + A_2\exp\left(-\frac{t}{\tau_2}\right) + B \qquad \text{Equation 6}$$

It is noticed that the double-exponential functions better describe the decay profiles of **1**. For example, the reduced χ^2 values of double-exponential functions are much closer to 1, which represents an ideal fitting.

The double-exponential decays of **1** suggest that there are two different fluorescence mechanisms in the emission of these compounds. We assign the relatively short-lived fluorescence (lifetime ≈ 2 ns) to the emission resulting from intramolecular charger transfer (ICT), and the

relatively long-lived fluorescence (lifetime ≈ 7 ns) to the emission resulting from twisted intramolecular charger transfer (TICT). TICT emission has much longer lifetime than ICT emission[19]; the twisting along the N—C axis at the 4-position of the 1, 8-naphthalimide fluorophore upon optical excitation is responsible for TICT emission.

The changes of ICT emission (blue), TICT emission (red), and the total emission (green) intensities of **1** over solvent viscosity are plotted in Figure S21.

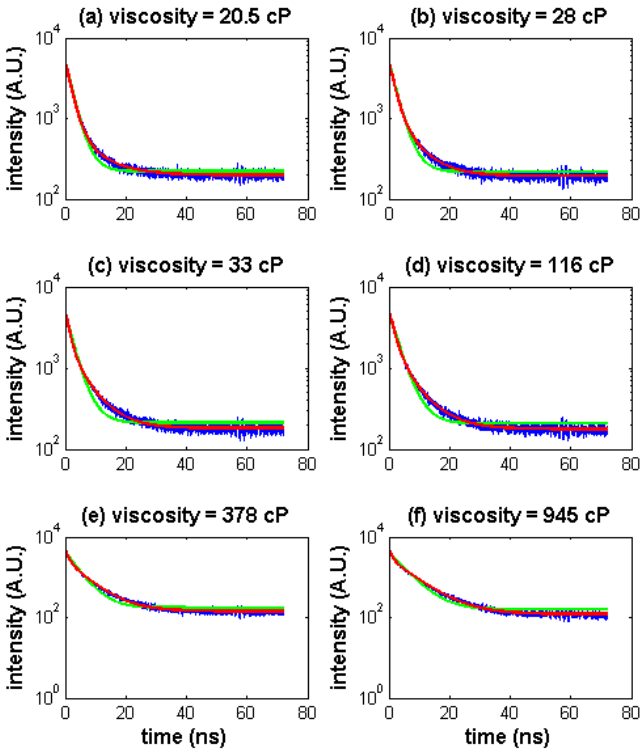

Figure S20. Normalized fluorescence decay curves of compound **1** in ethylene glycol and glycerol mixtures (**blue**: raw data; **green**: single-exponential best-fit; **red**: double-exponential best-fit).

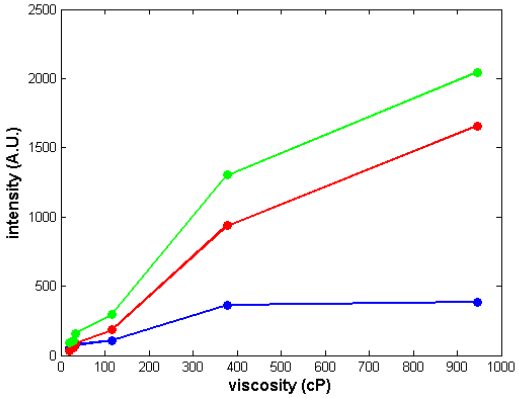

Figure S21. Fluorescence intensity changes of **1** over solvent viscosity (**red**: TICT emission; **blue**: ICT emission; and **green**: the total emission).

Table S8. Fitting parameters to experimental fluorescence decay curves of **1**.

	single-exponential decay					**double-exponential decay**										
viscosity	***A***	***τ* (ns)**	***B***	***reduced* χ^2**		***A*$_1$**	***A*$_2$**	***τ*$_1$ (ns)**	***τ*$_2$ (ns)**	***B***	***reduced* χ^2**	***a*$_1$%**[a]	***a*$_2$%**[b]	**fluorescence intensity (*I*)**	**ICT**[c]	**TICT**[d]
20.5 cP	4827.0	2.7	220.7	4.5		4230.9	812.6	2.1	6.8	201.4	1.3	62%	38%	90	55	35
28 cP	4716.3	2.9	217.5	6.3		3957.2	1053.9	2	6.9	192.9	1.3	52%	48%	109	57	52
33 cP	4292.8	3.1	211.2	9.5		3690	1018	2	8.2	181.8	1.3	47%	53%	159	74	84
116 cP	4474.6	3.5	206.4	8.0		3278.7	1600.2	2	6.9	177.6	1.3	37%	63%	293	109	184
378 cP	3957.5	4.2	175.1	11.8		2897	1731	1.9	8.2	136	1.4	28%	72%	1302	364	938
945 cP	3691.8	5.5	152.3	10.9		2515	2139	1.8	9.1	122.6	1.4	19%	81%	2045	386	1659

[a] The relative contribution of the short-lived ICT emission in the total emission; it is computed via $a_1\% = A_1\tau_1/(A_1\tau_1 + A_2\tau_2)$.

[b] The relative contribution of the long-lived TICT emission in the total emission; it is computed via $a_2\% = A_2\tau_2/(A_1\tau_1 + A_2\tau_2)$.

[c] The absolute contribution of the short-lived ICT emission in the total emission; it is computed via $ICT = a_1\% * I$, where *I* is the measured peak emission intensity in a given solvent.

[d] The absolute contribution of the long-lived TICT emission in the total emission; it is computed via $TICT = a_2\% * I$, where *I* is the measured peak emission intensity in a given solvent.

Additional Comments on Factors Controlling PET rates

The TICT promoted PET enhancement can be also rationalized both via the Rehm-Weller equation (Equation 7)[20-23] and the Marcus equation (Equation 8)[24].

Rehm-Weller equation computes the free energy of a PET reaction, ΔG_{ET}; a negative ΔG_{ET} suggests that PET is thermodynamically favorable. Assuming that $E(D^+/D)$, $E(A/A^-)$, and $\Delta E_{0,0}$ remain about the same in both the ICT and TICT states, a shorter distance between the donor and acceptor affords a larger electrostatic interaction ($-\frac{e^2}{4\pi\varepsilon R}$), and thus a greater driving force for PET to proceed.

Furthermore, according to the Marcus equation, a smaller distance between the donor and acceptor means a larger overlap matrix V, and larger $\exp\left[-\frac{(\Delta G_{ET}+\lambda)^2}{4\lambda k_B T}\right]$ term (due to a more negative ΔG_{ET}, assuming not in the inverted region); and the PET rate is thus higher.

$$\Delta G_{ET} = E(D^+/D) - E(A/A^{-1}) - \Delta E_{0,0} - \frac{e^2}{4\pi\varepsilon R} \qquad \text{Equation 7}$$

where $E(D^+/D)$ is the oxidation potential of the electron donor; $E(A/A^{-1})$ is the reduction potential of the electron acceptor; $\Delta E_{0,0}$ is the zero-zero transition energy; R is distance between the donor and acceptor.

$$k_{ET} = \left(\frac{4\pi^3}{\hbar^2 \lambda k_B T}\right)^{0.5} V^2 \exp\left[-\frac{(\Delta G_{ET}+\lambda)^2}{4\lambda k_B T}\right] \qquad \text{Equation 8}$$

where $\hbar$ is Planck's constant; k_B is the Boltzmann constant; T is the absolute temperature; λ is the reorganization energy; and V is the electronic coupling matrix.

The V term increases exponentially as the distance between the donor and acceptor decreases[25].

By the same token, as the 4-position substituent switches from the N-shaped conformer to the U-shaped conformer, the PET donor and acceptor in **1** become closer, resulting in a larger MO overlap; and it is not surprising that their PET rat rises substantially, by ~10 times according to our estimation.

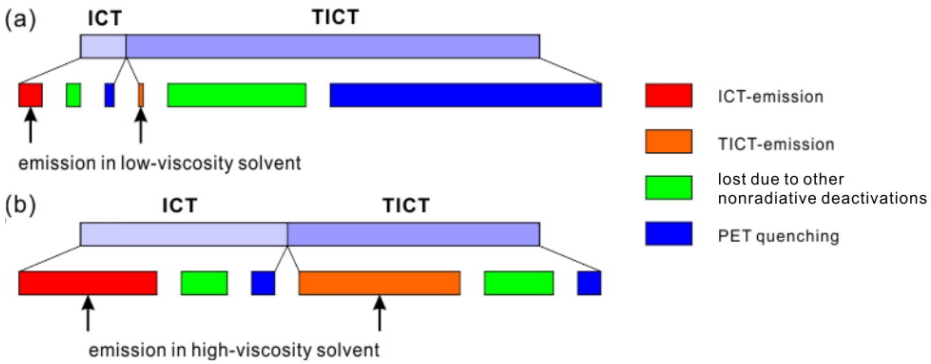

Figure S22. A schematic illustration of fluorescence enhancement of **1** as solvent viscosity increases, i.e., the TICT excited states becomes less dominant and quantum efficiencies of both

ICT and TICT emission rise due to constrained rotations to conformers prone to PET.

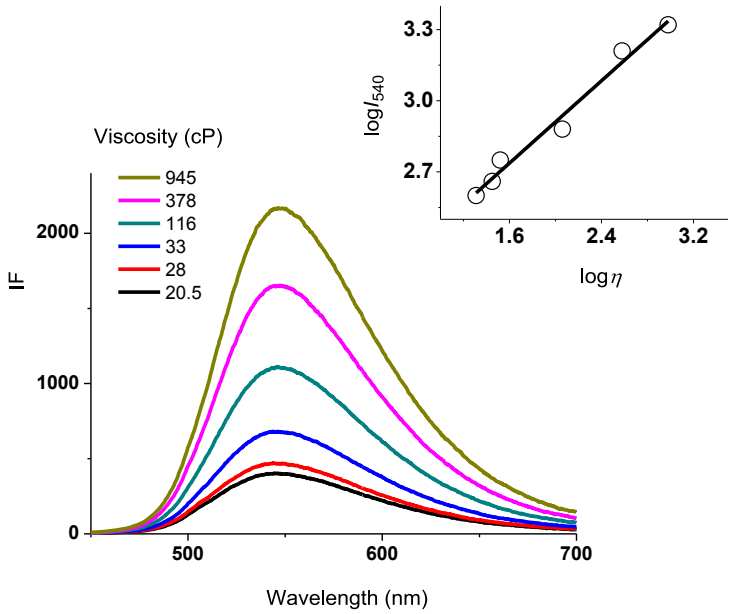

Figure S23. Fluorescent emission spectra of 10 μM **4** in ethylene glycol-glycerol mixtures with varied viscosity, excited at 440 nm. Inset: the linearity between logI_{540} and log η.

NMR Spectra of 1—3, 5, 7 and 8

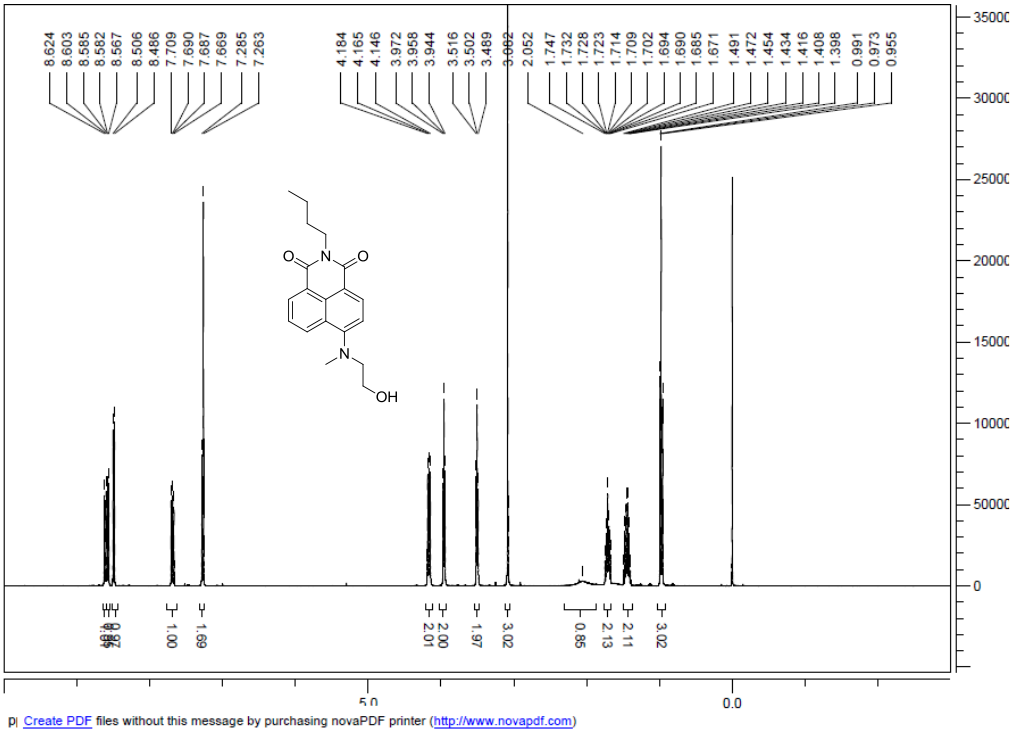

Figure S24. ^{1}H-NMR spectra of compound **6** in $CDCl_3$.

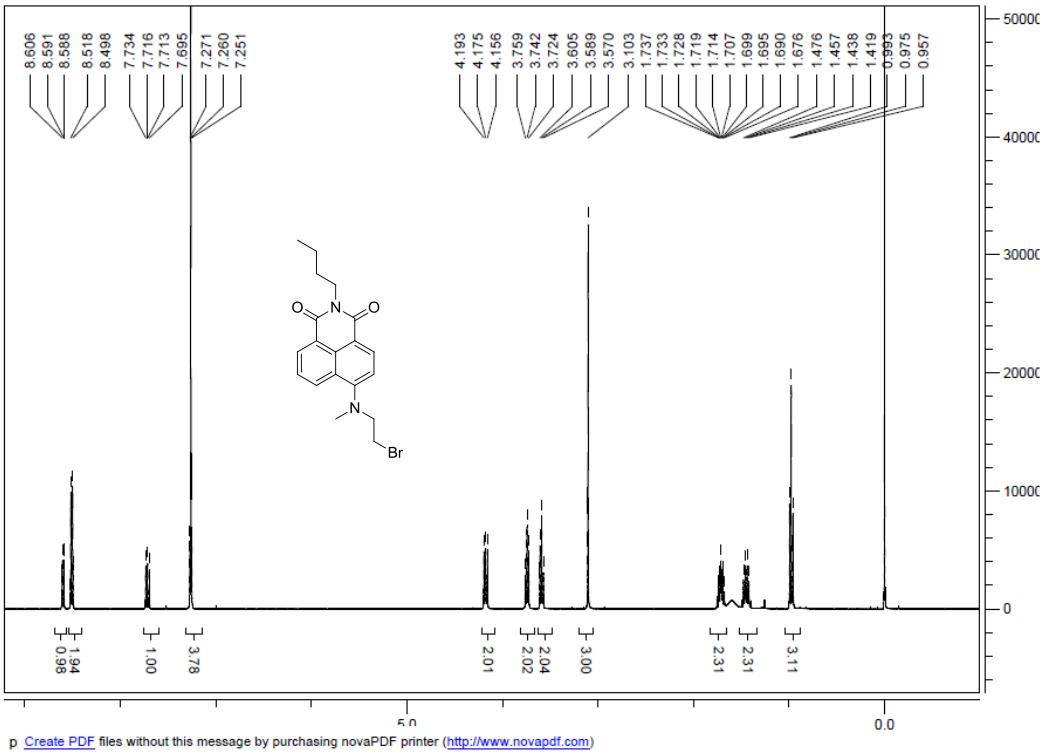

Figure S25. ^{1}H-NMR spectra of compound **7** in $CDCl_3$.

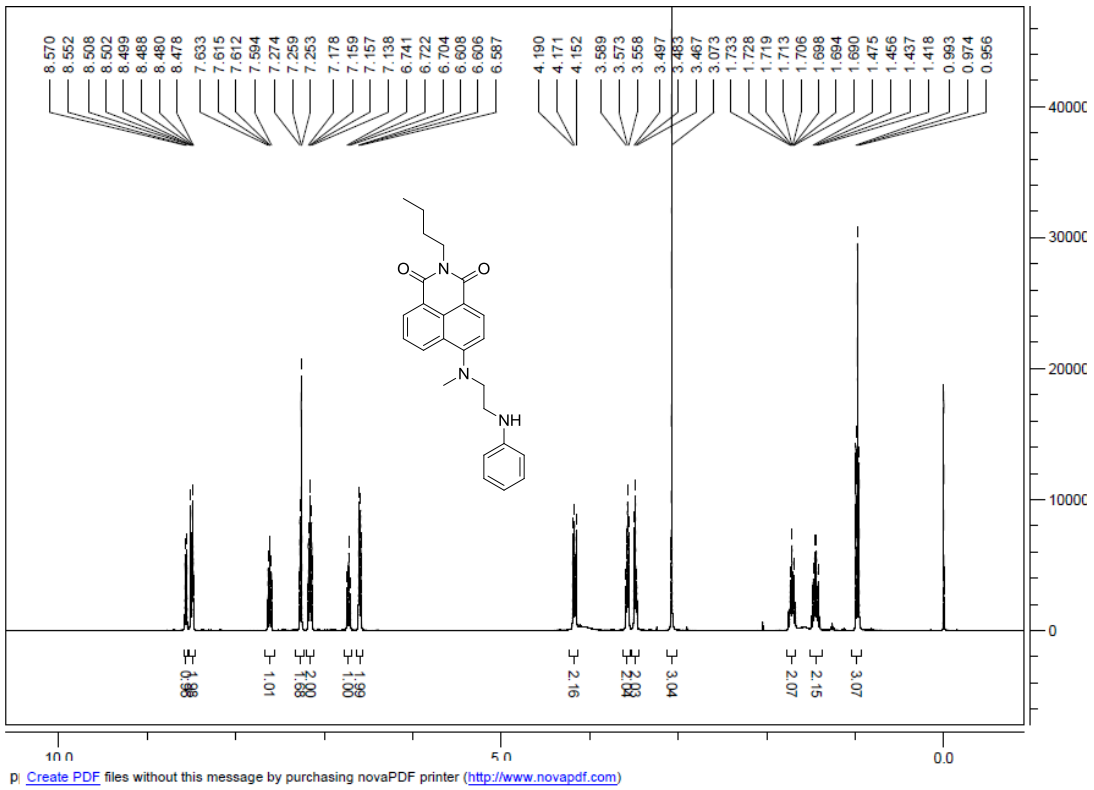

Figure S26. ^{1}H-NMR spectra of compound **3** in $CDCl_3$.

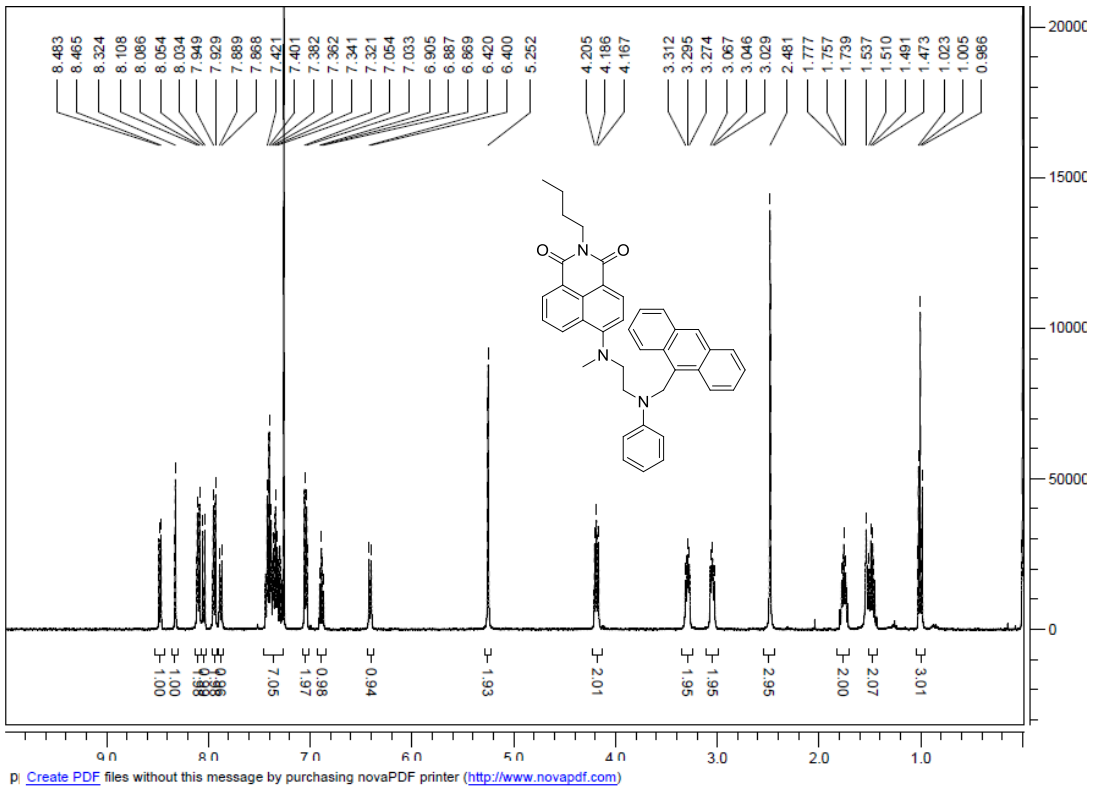

Figure S27. ^{1}H-NMR spectra of compound **1** in $CDCl_3$.

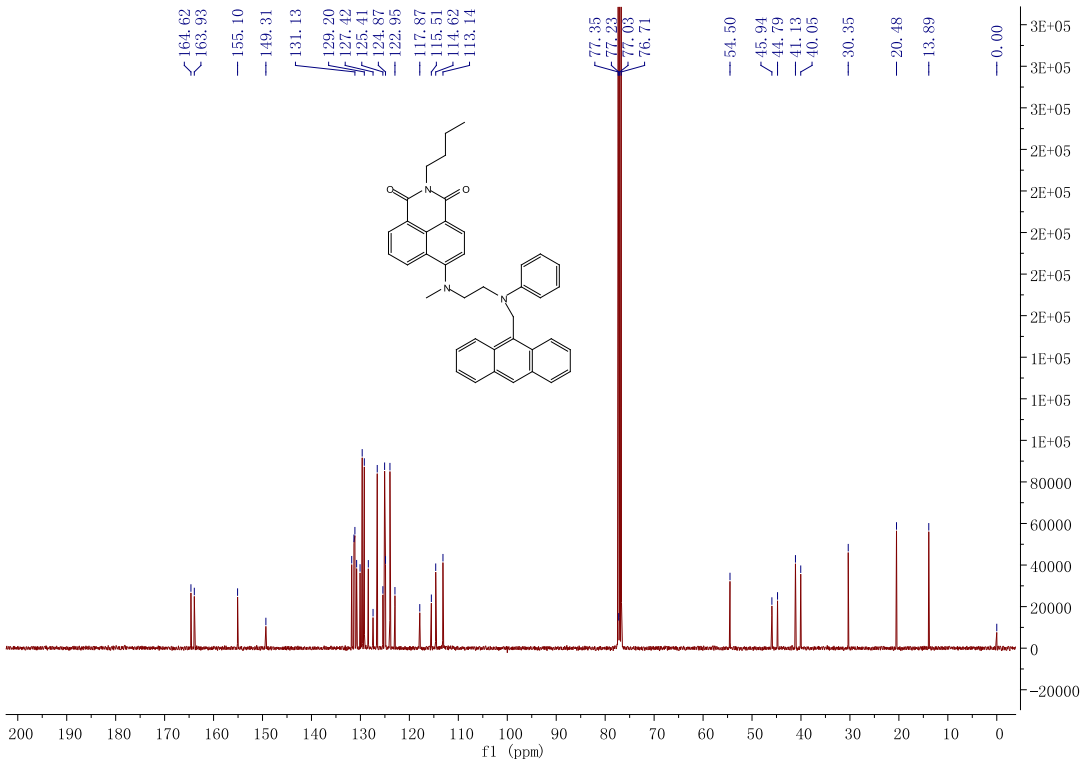

Figure S28. ^{13}C-NMR spectra of compound **1** in $CDCl_3$.

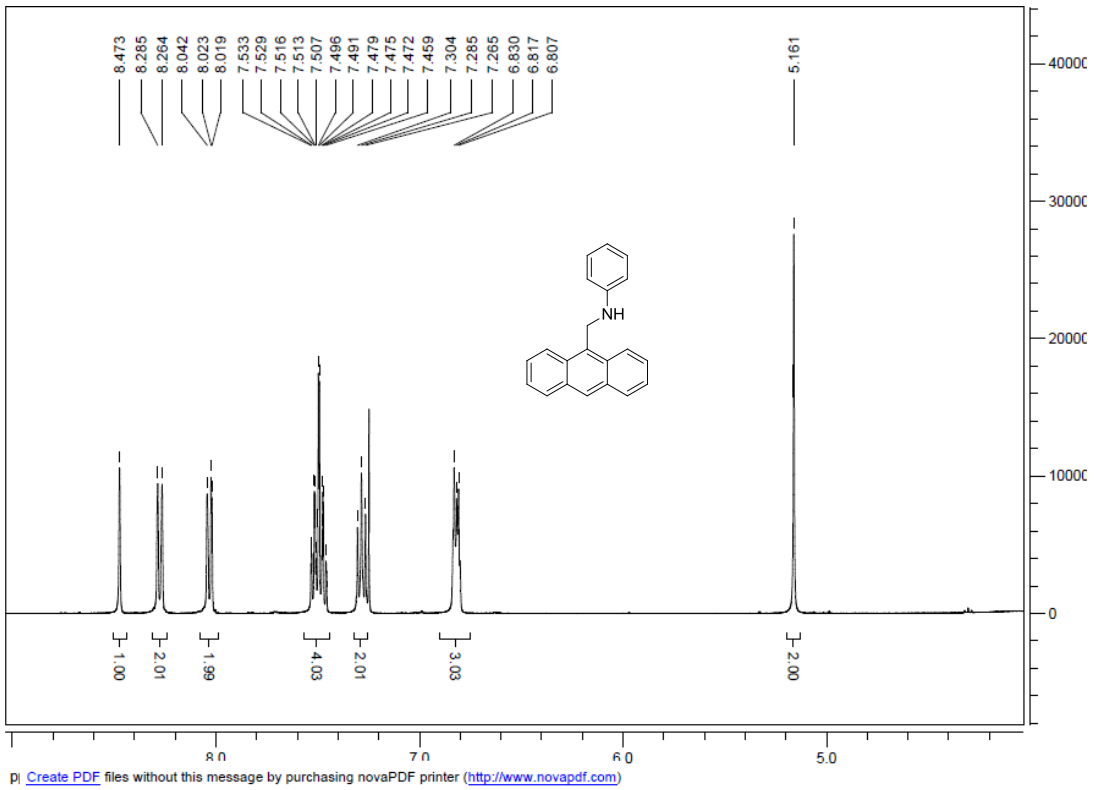

pl Create PDF files without this message by purchasing novaPDF printer (http://www.novapdf.com)

Figure S29. ^{1}H-NMR spectra of compound **2** in $CDCl_3$.

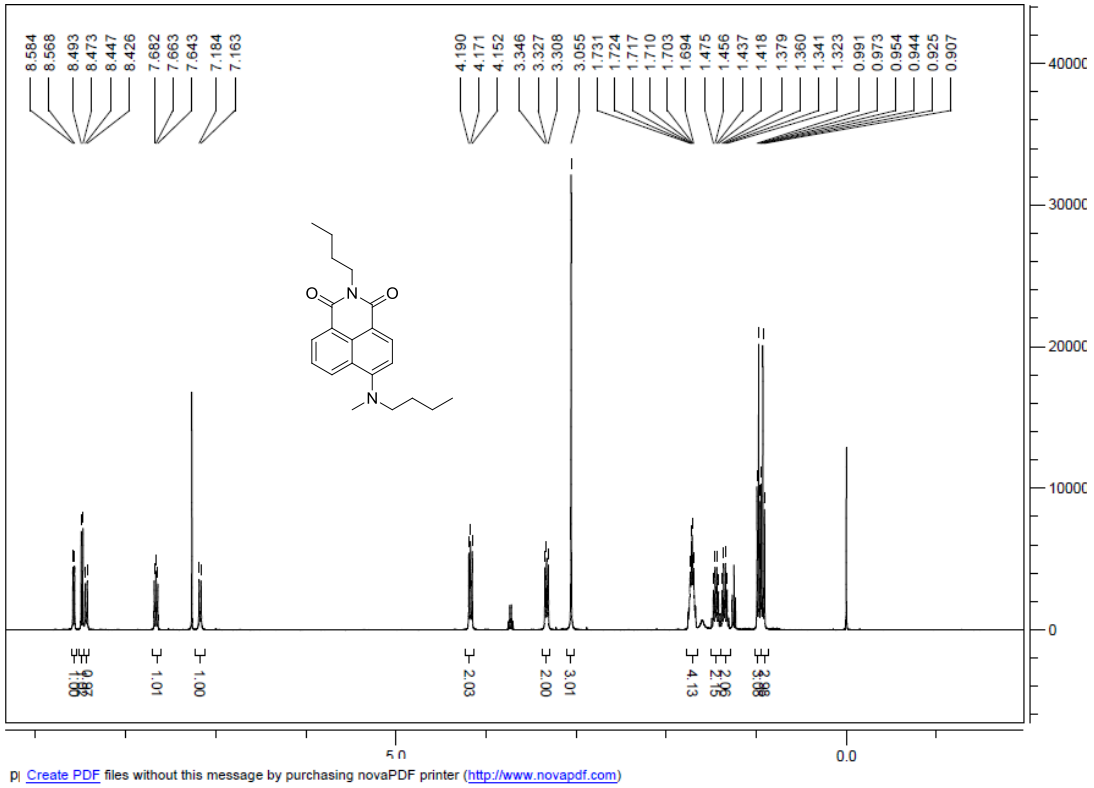

pl Create PDF files without this message by purchasing novaPDF printer (http://www.novapdf.com)

Figure S30. ^{1}H-NMR spectra of compound **4** in $CDCl_3$.

References

1 Jares-Erijman, E. A. & Jovin, T. M. FRET imaging. *Nat. Biotech.* **21**, 1387-1395 (2003).

2 Forster, T. & Hoffmann, G. Z. *Phys. Chem.* **75**, 63-76 (1971).

3 Gaussian 09 (Gaussian Inc., Wallingford, CT, 2009).

4 O'Boyle, N. M., Vandermeersch, T., Flynn, C. J., Maguire, A. R. & Hutchison, G. R. Confab-systematic generation of diverse low-energy conformers. *J. Cheminform.* **3**, 1-9 (2011).

5 Stewart, J. J. Optimization of parameters for semiempirical methods V: modification of NDDO approximations and application to 70 elements. *J. Mol. Model.* **13**, 1173-1213 (2007).

6 Stephens, P. J., Devlin, F. J., Chabalowski, C. F. & Frisch, M. J. Ab Initio Calculation of vibrational absorption and circular dichroism spectra using density functional fields. *J. Phys. Chem.* **98**, 11623-11627 (1994).

7 Becke, A. D. Density-functional thermochemistry. III. the role of exact exchange. *J. Chem. Phys.* **98**, 5648-5652 (1993).

8 Lee, C., Yang, W. & Parr, R. G. Development of the Colle-Salvetti correlation-energy formula into a functional of the electron density. *Phys. Rev. B* **37**, 785-789 (1988).

9 Binkley, J. S., Pople, J. A. & Hehre, W. J. Self-consistent molecular orbital methods. 21. Small split-valence basis sets for first-row elements. *J. Am. Chem. Soc.* **102**, 939-947 (1980).

10 Gordon, M. S., Binkley, J. S., Pople, J. A., Pietro, W. J. & Hehre, W. J. Self-consistent molecular-orbital methods. 22. Small split-valence basis sets for second-row elements. *J. Am. Chem. Soc.* **104**, 2797-2803 (1982).

11 Blake, A. J. *et al.* Structure analysis restrained by ab initio calculations: the molecular structure of 2, 5-dichloropyrimidine in gaseous and crystalline phases. *J. Phys. Chem.* **100**, 12280-12287 (1996).

12 Rassolov, V. A., Ratner, M. A., Pople, J. A., Redfern, P. C. & Curtiss, L. A. 6-31G* basis set for third-row atoms. *J. Comput. Chem.* **22**, 976-984 (2001).

13 Chipman, D. M. Reaction field treatment of charge penetration. *J. Chem. Phys.* **112**, 5558 (2000).

14 Miertus, S., Scrocco, E. & Tomasi, J. Electrostatic interaction of a solute with a continuum. A direct utilizaion of ab initio molecular potentials for the prevision of solvent effects. *Chem. Phys.* **55**, 117-129 (1981).

15 Bañuelos, J. *et al.* Photophysical study of new versatile multichromophoric diads and triads with BODIPY and polyphenylene groups. *J. Phys. Chem. A* **112**, 10816-10822 (2008).

16 Kennedy, D. P., Kormos, C. M. & Burdette, S. C. FerriBright: A rationally designed fluorescent probe for redox active metals. *J. Am. Chem. Soc.* **131**, 8578-8586 (2009).

17 Lu, H. *et al.* Experimentation and theoretic calculation of a BODIPY sensor based on photoinduced electron transfer for ions detection. *J. Phys. Chem. A* **113**, 14081-14086 (2009).

18 Salman, H. *et al.* Sensitive and selective PET-based diimidazole luminophore for ZnII ions: a structure-activity correlation. *Inorg. Chem.* **45**, 5315-5320 (2006).

19 Rettig, W. & Klock, A. Intramolecular fluorescence quenching in aminocoumarines. Identification of an excited state with full charge separation. *Can. J. Chem.* **63**, 1649-1653 (1985).

20 Rehm, D. & Weller, A. Kinetics of fluorescence quenching by electron and H-atom transfer. *Isr. J. Chem* **8**, 259-272 (1970).

21 Kavarnos, G. J. & Turro, N. J. Photosensitization by reversible electron transfer: theories, experimental evidence, and examples. *Chem. Rev.* **86**, 401-449 (1986).

22 Cody, J., Mandal, S., Yang, L. & Fahrni, C. J. Differential tuning of the electron transfer parameters in 1, 3, 5-Triarylpyrazolines: a rational design approach for optimizing the contrast ratio of fluorescent probes. *J. Am. Chem. Soc.* **130**, 13023-13032 (2008).

23 Lakowicz, J. R. *Principles of fluorescence spectroscopy*. (Springer, 2009).

24 Marcus, R. A. Electron transfer reactions in chemistry. Theory and experiment. *Rev. Mod. Phys.* **65**, 599-610 (1993).

25 Balzani, V. *Electron Transfer in Chemistry: Principles and theories, methods and techniques*. (Wiley-VCH, 2001).